Direct Observation of Density-Gradient Effects in Harmonic Generation from Plasma Mirrors

S. Kahaly,[1] S. Monchocé,[1] H. Vincenti,[1] T. Dzelzainis,[2] B. Dromey,[2] M. Zepf,[2,3] Ph. Martin,[1] and F. Quéré[1,*]

[1]*Service des Photons, Atomes et Molécules, Commissariat à l'Energie Atomique, DSM/IRAMIS, CEN Saclay, 91191 Gif sur Yvette, France*

[2]*Centre for Plasma Physics, School of Mathematics and Physics, Queen's University Belfast, Belfast BT7 1NN, United Kingdom*

[3]*Helmholtz Institut Jena, 07743 Jena, Germany*

(Received 7 December 2012; published 22 April 2013)

High-order harmonics and attosecond pulses of light can be generated when ultraintense, ultrashort laser pulses reflect off a solid-density plasma with a sharp vacuum interface, i.e., a plasma mirror. We demonstrate experimentally the key influence of the steepness of the plasma-vacuum interface on the interaction, by measuring the spectral and spatial properties of harmonics generated on a plasma mirror whose initial density gradient scale length L is continuously varied. Time-resolved interferometry is used to separately measure this scale length.

DOI: 10.1103/PhysRevLett.110.175001 PACS numbers: 52.38.−r, 42.65.Ky, 52.27.Ny, 52.65.Rr

Laser technology now makes it possible to generate femtosecond (fs) laser pulses with peak intensities such that the motion of electrons in the laser field is relativistic. Plasma mirrors (PMs), created when such ultraintense pulses are focused on a solid target, can be considered as test beds of this extreme regime of laser-plasma interaction [1,2]. They specularly reflect the incident laser light, and their nonlinear response to the intense field can lead to high-order harmonics generation (HHG) of the incident laser frequency in this reflected beam [1,3]. This constitutes a fine *in situ* probe of the interaction to investigate the underlying physics [4–7]. In addition, it has long raised interest as a source of coherent short-wavelength radiation [1], revived recently by the prospect of producing intense attosecond pulses of light [8–11].

The recent improvements in the temporal contrast of ultraintense fs pulses have allowed significant progress in the understanding of HHG on plasma mirrors. In particular, two distinct generation mechanisms have been identified, in simulations as well as in experiments [3]. Both are associated with the energetic electron population that is coherently driven at the plasma surface by the laser field, predominantly by its p-polarized component. As these electrons are pulled out of the plasma by the laser, during a fraction of the laser optical cycle, they can induce a Doppler upshift on the reflected field, leading to the emission of high frequencies, temporally bunched in the form of an attosecond burst. When the laser field changes sign later in the optical cycle, these electrons get pushed back toward the target. A fraction of them form attosecond charge bunches as they penetrate the dense plasma, where they impulsively excite collective electron oscillations. In the inhomogeneous plasma formed by the density gradient at the plasma-vacuum interface, these high-frequency oscillations can emit light, again in the form of an attosecond burst, through linear mode conversion. These two different elementary processes, respectively called relativistic oscillating mirror (ROM) [2,12] and coherent wake emission (CWE) [13], repeat every laser cycle resulting in the emission of attosecond pulse trains, associated with spectra of harmonics of the laser frequency.

The relative weight of these two mechanisms in the total harmonic signal is most often considered to be entirely determined by the laser intensity. Since ROM is based on a Doppler effect, it becomes efficient only when the velocity of outgoing electrons approaches c [2,12]. This typically requires a normalized vector potential $a_0 = eA_L/mc \geq 1$ for the laser field (A_L amplitude of laser vector potential, e and m electron charge and mass), which corresponds to intensities exceeding $\sim 2 \times 10^{18}$ W/cm^2 for an 800 nm laser field. In contrast, electron energy plays little role in CWE, which has thus been observed experimentally for intensities as low as a few 10^{15} W/cm^2 [13].

A less evident, but equally crucial physical parameter is the steepness of the density gradient at the plasma-vacuum interface, precisely where HHG occurs. While there are some experimental indications [14–17], clear evidence of the influence of this parameter has so far relied on simulations [3,16]. In this Letter, we present a direct, quantitative experimental investigation of the influence of the interface steepness on HHG from PMs, and demonstrate the dramatic and contrasted dependences of the HHG mechanisms on this parameter.

The experiment is carried out using the 100 terawatt UHI100 Ti:sapphire laser (25 fs pulses, central wavelength $\lambda = 800$ nm) at IRAMIS (Commissariat à l'Energie Atomique). The contrast of the beam, initially better than 10^8 at times $t \geq 10$ ps before the main pulse, is raised by 4 orders of magnitude by using a double plasma mirror setup [18]. A weak prepulse is then introduced at an adjustable delay τ before the main pulse, to ionize the target and initiate controlled plasma expansion, leading to an exponential [19] density gradient at the plasma-vacuum interface, $n \propto \exp(x/L)$. When the main pulse arrives, it thus interacts

with a target with an initial density gradient, whose scale length L can be continuously tuned by changing τ. Both pulses are p polarized and incident at 55° on the target.

A simple and stable scheme is used to introduce this controlled prepulse (Fig. 1). A 1/2 inch diameter mirror (M_1) is placed on an edge of the main laser beam (3 inches diameter), at a variable distance δ in front of a mirror (M_2) used for the transport of the main beam [Fig. 1(a)]. The small fraction of the main beam intercepted by M_1 produces the required prepulse. M_1 and M_2 are made exactly parallel, so that the main and prepulse beams are focused at the same position on the target by an off-axis parabola ($f = 200$ mm). Due to its smaller diameter, the prepulse beam produces a larger focal spot than the main beam [Fig. 1(b)]: the density gradient that it creates can thus be considered as homogeneous all across the HHG source. Its peak intensity is $\sim 10^{16}$ W/cm^2, which is high enough to strongly ionize the surface of the silica target used in the experiment.

To be able to reach zero or even negative delays (i.e., no prepulse) between the two beams, the prepulse reflects off the metal-coated rear face of M_1. As a result, it propagates twice through the $d = 2$ mm thick glass substrate of M_1, accumulating a retardation of $\Delta\tau \propto 2d(1/v_g - 1/c)$ ($v_g \approx 2c/3$ group velocity in glass) with respect to the main pulse. Zero delay can then be obtained very easily when $\delta = d(c/v_g - 1) \approx d/2$. The front face of M_1 is antireflection coated, and slightly tilted with respect to the back face, to avoid the creation of a parasite prepulse.

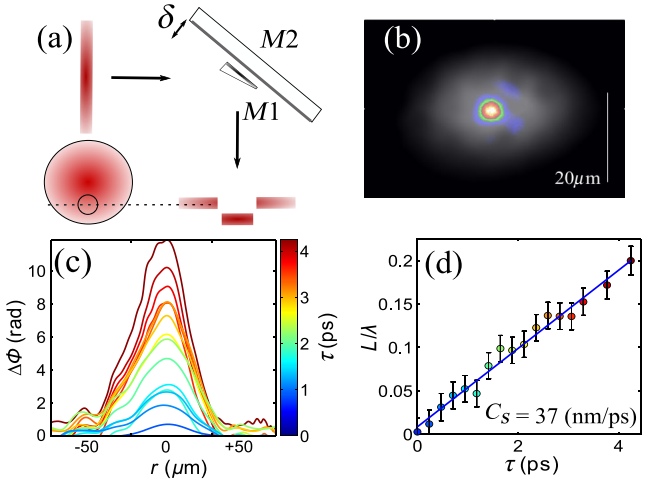

FIG. 1 (color online). (a) Experimental scheme for density gradient control. Two mirrors M_1 and M_2 are used to separate the prepulse and main pulse in time, before the focusing parabola. Side and front views of the full laser beam are shown in red. (b) Resulting intensity distributions of the prepulse beam (gray scale) and main beam (bright central spot) at the focus. (c) Temporal evolution of the spatially resolved phase shift induced on the FDI probe pulse by the plasma expansion triggered by the prepulse. (d) Temporal evolution of the density gradient scale length L at the center of the prepulse beam, as deduced from the measured phase shifts.

The initial density gradient L is determined as a function of delay τ, by measuring the phase shift it induces on a probe beam, using time-resolved frequency-domain interferometry (FDI) [20] in the spatial-shearing configuration. For these measurements, the scheme of Fig. 1(a) is again used, but now most of the main beam is blocked, and a weak probe ($I \approx 10^9$ W/cm^2) is obtained by selecting a very small fraction of this beam with a 200 μm diaphragm. Figure 1(c) shows the spatially resolved phase shift, $\Delta\Phi(r, \tau)$ induced by the expanding plasma on the FDI probe, where r is the transverse distance from the center of the laser focus ($r = 0$) at the target plane. This gives the displacement of the critical density surface with respect to the initial target plane at each delay τ, from which the gradient scale length L can be deduced. We observe that L varies linearly with τ [Fig. 1(d)], and the slope of the linear fit gives an ion sound speed of $C_s = dL/d\tau = 37$ nm/ps at the center of the prepulse beam. This value is used to make the correspondence between the delay and the gradient scale length for the rest of the experiment.

The harmonic beam produced by the main laser pulse on the gradient-controlled plasma mirror is spectrally dispersed using a 1200 lines/mm varied line spacing concave extreme ultraviolet grating (Shimadzu 30-002). This provides angularly resolved harmonic spectra $S(\omega, \theta)$, which are detected using a large 69 mm × 88 mm rectangular microchannel plate coupled to a phosphor screen, imaged on a CCD camera. This large detector made it possible to measure the full angular profile of the harmonic beam (detection window of ±70 mrad).

The first series of measurements were carried out slightly below the relativistic interaction limit, by placing a 1 inch aperture in the main beam, leading to a 15.8 μm focal spot on the target and a peak intensity of $\sim 1 \times 10^{18}$ W/cm^2 ($a_0 \approx 0.7$). The prepulse beam passed through a separate hole in the aperture and was thus unaffected. In this regime, the contribution of CWE to the HHG signal is generally assumed to dominate over ROM. In contrast, we find that this balance strongly depends on the density gradient: the harmonic signal can be totally dominated either by CWE, for the shortest scale lengths ($L/\lambda \leq 0.02$), or by ROM, for larger scale lengths ($L/\lambda \geq 0.04$), as observed numerically in Ref. [16].

There are two main signatures that enable one to distinguish the CWE and ROM contributions to the HHG signal. The first one is in the spectral domain: CWE can only generate harmonics up to the maximum plasma frequency $\omega_p^{\max}$ of the plasma mirror ($\approx 20\omega_L$ for fully ionized silica at the initial solid density), while no such limitation applies to ROM. As a result, any harmonic frequency above $\omega_p^{\max}$ can only be attributed to ROM. The second signature is in the spatial domain: CWE produces harmonics with a larger divergence than those originating from ROM. This is because the CWE harmonic phase has a stronger dependence on laser intensity than ROM one [21]. Combined

with the nonuniform spatial intensity profile of the laser at focus, this leads to a spatially curved harmonic wavefront in the source plane, which considerably increases the CWE beam divergence compared to ROM.

We now examine the experimental results, with these two signatures in mind. Figures 2(a)–2(c) show the angularly resolved harmonic spectra $S(\omega, \theta)$ measured for three different density gradients. The complete evolution of $S(\omega, \theta)$ with scale length L is presented in Ref. [22]. As L is increased, there is a complete transition from CWE to ROM, for all observed harmonic orders, which is revealed by (i) a dramatic reduction of the harmonic beam divergence for all measured orders and (ii) a simultaneous change in the highest observed harmonic frequency, which moves from $\omega_p^{\max}$ initially, to slightly higher values ($\approx 25\omega_L$). When both mechanisms coexist, their contributions to the harmonic signal can interfere [3]. This can explain the clear interference fringes that are observed experimentally in the transition regime [see zoom in Fig. 2(e)].

Since the measured signal $S(\omega, \theta)$ only corresponds to a 1D lineout out of a 2D spatial distribution, the total spatially integrated emission from the plasma mirror, $S'(\omega)$, is given by $S'(\omega) \propto \int S(\theta, \omega)\theta d\theta$, where θ is the propagation angle. Figures 2(d)–2(f) show the evolution of $S'(\omega)$ for three harmonic orders, below and above $\omega_p^{\max} = 20\omega_L$. Above $\omega_p^{\max}$ [Fig. 2(f)], the harmonic signal only exceeds the detection threshold for $L/\lambda \geq 0.02$, implying a better efficiency of ROM for density gradients that are not too sharp. In contrast, below $\omega_p^{\max}$ [Fig. 2(d)], $S'(\omega)$ first strongly drops up to $L/\lambda \approx 0.03$, and then keeps decreasing but at a much slower pace. According to our previous discussion, the first part of this curve (gray area) is dominated by CWE, whose efficiency decreases with L. In the second part (white area), the signal is due to ROM, whose efficiency only slowly decreases for $L/\lambda \gtrsim 0.02$, as observed in Fig. 2(f). Thus we see that in this intensity regime, much higher overall efficiencies can be achieved with CWE than with ROM using very short gradients, at the expense of a larger beam divergence.

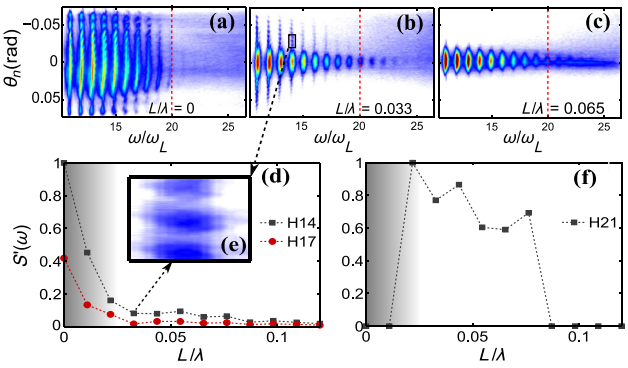

FIG. 2 (color online). Effect of the initial gradient scale length L at moderate laser intensity ($a_0 \approx 0.7$). Upper row: measured angularly resolved harmonic spectra for three different values of L. The lower graphs show the evolution of the total emission $S'(\omega)$ for three different harmonic orders, below (d) and above (f) the maximum plasma frequency $\omega_p^{\max}$ of fully ionized silica ($\approx 20\omega_L$). Each point corresponds to a single laser shot. Inset (e) shows a zoom on fringes observed in (b), right at the transition between CWE and ROM (see arrows), attributed to interferences between the harmonic signals associated with these two mechanisms.

This interpretation of the experimental observations is clearly supported by 2D particle-in-cell (PIC) simulations carried out under comparable physical conditions. Figure 3 presents angularly resolved harmonic spectra $S(\omega, \theta)$ obtained from such PIC simulations. In these simulations, the harmonic signal can be unambiguously associated predominantly with CWE for short gradients [Fig. 3(a)], and with ROM for long gradients [Fig. 3(b)], through a spatiotemporal analysis of the reflected field and plasma density, as was demonstrated in Ref. [13]. Like in the experiment, this transition results in a dramatic reduction of the harmonic beam divergence with increasing L.

We now move to a much higher laser intensity range, which is of great interest for the generation of intense attosecond pulses [23,24]. To this end, we focus the entire main beam onto a spot size of 4.7 μm (FWHM) using an adaptive optics system, reaching a peak intensity of $\simeq 5 \times 10^{19}$ W/cm^2 ($a_0 \simeq 4.9$). We observe that longer gradients lead to a significant increase of ROM signal and to an extension of the spectral cutoff. This is illustrated in Fig. 4, where the angularly resolved harmonic spectra $S(\omega, \theta)$ measured without (a) and with (b) prepulse are compared. Figure 4(c) shows the variation of the spatially integrated signal $S'(\omega)$ with L, for three harmonic orders above $\omega_p^{\max}$.

A striking feature is that even at this intensity, CWE has a comparable efficiency to ROM for very sharp gradients [Fig. 4(a)]. As the density gradient is increased [Fig. 4(b)], the CWE signal drops, whereas ROM signal quickly rises, up to $L/\lambda \approx 0.06$, and then grows at a slower pace [Fig. 4(c)]. As a result, ROM contribution totally dominates that of CWE over the whole observed spectral range as soon as $L/\lambda \geq 0.025$. The relative gain in signal is stronger for the two highest orders of Fig. 4(c),

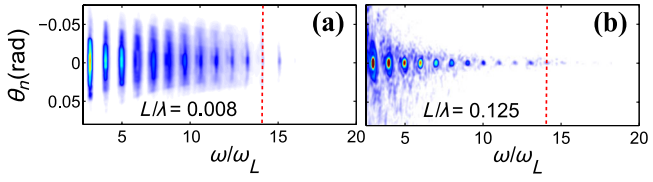

FIG. 3 (color online). Angularly resolved harmonic spectra obtained from 2D PIC simulations (CALDER code) for two different values of L, at the onset of the relativistic interaction regime ($a_0 = 0.9$). All physical parameters are comparable to those of the experiment of Fig. 2 except for the maximum plasma density, which is $n_e^{\max} = 200n_c$ (n_c critical plasma density for the laser), leading to a maximum plasma frequency (and hence a CWE cutoff) of $\sqrt{n_e^{\max}/n_c} \times \omega_L \approx 14\omega_L$.

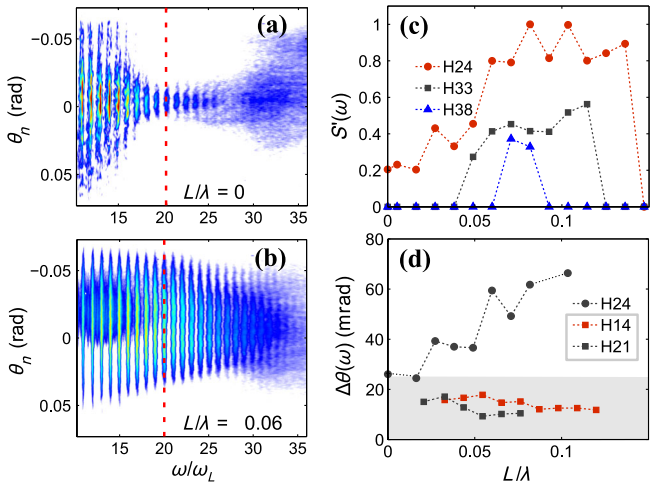

FIG. 4 (color online). Effect of the initial gradient scale length L at maximum laser intensity ($I = 5 \times 10^{19}$ W/cm^2, $a_0 \simeq 4.9$). (a),(b) Measured angularly resolved harmonic spectra for two different values of L/λ, 0 in (a) (no prepulse) and 0.06 in (b). Graph (c) shows the evolution of the total emission $S'(\omega)$ for three different harmonic orders above the 20th harmonic. In (d), the divergence of the 24th harmonic is plotted as a function of L. For comparison, this graph also shows the divergences of two harmonics (gray region) in the moderate intensity regime of Fig. 2, for gradients where ROM dominates the signal. Each point corresponds to a single laser shot.

indicating that the extent of the harmonic spectrum increases with L.

These studies in two different intensity regimes highlight the contrasted dependences of CWE and ROM with respect to the gradient scale length. This result is consistent with 1D PIC simulations [3,16]. For CWE, these simulations predict first a fast rise in signal, from a steplike interface, where no mode conversion and hence no CWE can occur, to very sharp density gradients where the efficiency is optimum, followed by a slower decrease [3]. In our experiment, we only observe the second part of this curve. This is because, even in the absence of the prepulse ($\tau \leq 0$), plasma expansion during the main pulse leads to a finite density gradient δL at the peak of this pulse, which prevents us from reaching sharper gradients during the interaction. This also explains why the CWE signal does not vanish for $L = 0$ in Figs. 2(a) and 4(a): L is the initial density gradient at the onset of the interaction, not the actual one at the peak of the main pulse. The high contrast of the main pulse ensures that this affects our measurements only for the smallest values of L. This is why the optimum of ROM harmonics appears at similar scale lengths for both low and high peak intensity cases.

Qualitatively, the decrease of the CWE signal with L observed in our experiment is due to two reasons. First, the trajectory crossings of laser-accelerated electrons occur efficiently only over a small range of distances from the critical density surface (Fig. 9 in Ref. [3]), which is almost independent of the gradient scale length. As L increases, electron bunching thus progressively occurs in regions of the plasma of lower and lower densities, contributing to the reduction of the signal in the highest CWE harmonic orders (corresponding to high plasma densities). Second, the conversion of plasma waves into light is also optimal for rather short gradients ($L/\lambda \approx 0.02$) [3].

In contrast, in the case of ROM, 1D PIC simulations predict an increase of efficiency for increasing L, followed by a progressive saturation. Qualitatively, this is because longer gradients are observed to lead to higher Lorentz factors for outgoing electrons, and hence the generation of higher harmonic orders. This can be attributed to the smaller restoring force exerted by the ion background against the laser field for softer gradients. This behavior is broadly consistent with our experimental findings. However, in both intensity regimes, we eventually observe a sharp drop of the harmonic signal for $L/\lambda \gtrsim 0.1$ [Figs. 2(f) and 4(c)]. Such a decrease does not occur in 1D simulations [3,17], but we do observe it in 2D simulations. Further investigations with 2D codes will be required to explain this behavior.

While the dependences of the efficiencies with L are similar in the moderate and high intensity regimes, a very distinct difference is the evolution of ROM beam divergence with L, as illustrated in Fig. 4(d). At $a_0 \simeq 0.7$, ROM harmonic divergence hardly changes with L (gray area), whereas at $a_0 \simeq 4.9$, it grows approximately linearly with L (white area). Previous studies [25] have shown that at high intensities ($a_0 \sim 3$), this divergence is mostly determined by the curvature of the plasma mirror surface, induced by the spatially inhomogenous radiation pressure exerted by the laser field as it reflects. This imposes a curvature on the wave fronts of ROM harmonics, which increases their divergence, akin to the intensity-dependent phase of the CWE harmonics. As in the CWE case, it can in principle be compensated by slightly defocusing the laser on the target [21]. This effect is intuitively expected to get stronger for longer gradients (i.e., softer plasmas), as confirmed by PIC simulations [25]. Our observation of ROM divergence growth with L in the high intensity case is thus consistent with a predominant influence of the plasma mirror curvature. In the lower intensity case, this influence becomes negligible, and the divergence is mostly determined by diffraction. The slight decrease in divergence with L might then be attributed to an increase in the harmonic source size.

In the geometrical limit where the mirror curvature totally dominates diffraction, the measured divergence $\Delta\theta$ can actually be exploited to estimate the denting of the plasma. In this limit, $\Delta\theta = w_q/f$, where w_q is the source diameter of harmonic q, and f the focal length of the curved plasma mirror. A simple geometrical calculation shows that $f = \cos\theta w_L^2/2\zeta$, where $w_L = 4.7$ μm is the laser focal spot diameter, θ the incidence angle, and ζ the denting of the plasma surface. Using a ratio of $w_q = 0.5 w_L$ for $q = 24$

(obtained from PIC simulations) leads to $f = 33$ μm and $\zeta \approx 150$ nm for the longest gradient of Fig. 4, which is consistent with what is obtained in PIC simulations [25].

In conclusion, we demonstrate that by varying the gradient scale length it is possible to choose either the CWE or ROM mechanism to generate HHG, even at a subrelativistic ($a_0 \lesssim 1$) laser intensity. In the transition regime, harmonics from the two different mechanisms interfere. This might be exploited in future experiments to determine the difference in the spatiospectral phase between CWE and ROM harmonics. In the strongly relativistic regime, larger values of L lead to optimized ROM production efficiency. Density gradient control, for which we have introduced a simple experimental scheme, will thus be essential for both the understanding and the optimization of HHG from plasma mirrors.

We gratefully acknowledge F. Réau, O. Tcherbakoff, and P. d'Oliveira for the laser operation and optimization. The research leading to these results has received funding from the European Research Council (ERC Grant Agreement No. 240013) and LASERLAB-EUROPE (Grant Agreement No. 228334). The simulations were performed by using HPC resources from GENCI-CCRT/CINES (Grant No. 2012-056057). S. Kahaly and S. Monchocé contributed equally to this work.

*fabien.quere@cea.fr

[1] U. Teubner and P. Gibbon, Rev. Mod. Phys. **81**, 445 (2009).
[2] C. Thaury *et al.*, Nat. Phys. **3**, 424 (2007).
[3] C. Thaury and F. Quéré, J. Phys. B **43**, 213001 (2010).
[4] C. Thaury, H. George, F. Quéré, R. Loch, J.-P. Geindre, P. Monot, and Ph. Martin, Nat. Phys. **4**, 631 (2008).
[5] A. Borot, A. Malvache, X. Chen, A. Jullien, J.-P. Geindre, P. Audebert, G. Mourou, F. Quéré, and R. Lopez-Martens, Nat. Phys. **8**, 416 (2012).
[6] M. Tatakaris *et al.*, Nature (London) **415**, 280 (2002).
[7] I. Watts, M. Zepf, E. Clark, M. Tatarakis, K. Krushelnick, A. Dangor, R. Allott, R. Clarke, D. Neely, and P. Norreys, Phys. Rev. Lett. **88**, 155001 (2002).
[8] Y. Nomura *et al.*, Nat. Phys. **5**, 124 (2008).
[9] G. Sansone, L. Poletto, and M. Nisoli, Nat. Photonics **5**, 655 (2011).
[10] P. Heissler *et al.*, Phys. Rev. Lett. **108**, 235003 (2012).
[11] J. Wheeler, A. Borot, S. Monchocé, H. Vincenti, A. Ricci, A. Malvache, R. Lopez-Martens, and F. Quéré, Nat. Photonics **6**, 829 (2012).
[12] B. Dromey *et al.*, Nat. Phys. **2**, 456 (2006).
[13] F. Quéré, C. Thaury, P. Monot, S. Dobosz, Ph. Martin, J.-P. Geindre, and P. Audebert, Phys. Rev. Lett. **96**, 125004 (2006).
[14] M. Zepf *et al.*, Phys. Rev. E **58**, R5253 (1998).
[15] A. Tarasevitch, A. Orisch, D. von der Linde, Ph. Balcou, G. Rey, J.-P. Chambaret, U. Teubner, D. Klöpfel, and W. Theobald, Phys. Rev. A **62**, 023816 (2000).
[16] A. Tarasevitch, K. Lobov, C. Wünsche, and D. von der Linde, Phys. Rev. Lett. **98**, 103902 (2007).
[17] C. Rödel *et al.*, Phys. Rev. Lett. **109**, 125002 (2012).
[18] A. Lévy *et al.*, Opt. Lett. **32**, 310 (2007).
[19] Y. B. Zeldóvich and Y. P. Raizer, *Physics of Shock Waves and High-Temperature Hydrodynamic Phenomena* (Dover Publications, New York, 2002).
[20] J. P. Geindre, P. Audebert, A. Rousse, F. Falliès, J. C. Gauthier, A. Mysyrowicz, A. Dos Santos, G. Hamoniaux, and A. Antonetti, Opt. Lett. **19**, 1997 (1994).
[21] F. Quéré, C. Thaury, J.-P. Geindre, G. Bonnaud, P. Monot, and Ph. Martin, Phys. Rev. Lett. **100**, 095004 (2008).
[22] See Supplemental Material at http://link.aps.org/supplemental/10.1103/PhysRevLett.110.175001 for movie showing continuous transition from CWE to ROM regime of high order harmonic generation with varying plasma mirror density gradient.
[23] G. D. Tsakiris, K. Eidmann, J. Meyer-ter-Vehn, and F. Krausz, New J. Phys. **8**, 19 (2006).
[24] B. Dromey *et al.*, Phys. Rev. Lett. **99**, 085001 (2007).
[25] B. Dromey *et al.*, Nat. Phys. **5**, 146 (2009).